Protein-Protein Interaction on Lysozyme Crystallization Revealed by Rotational Diffusion Analysis

Daisuke Takahashi,* Etsuko Nishimoto,* Tadashi Murase,† and Shoji Yamashita*

*Institute of Biophysics, Faculty of Agriculture, Kyushu University, 6-10-1 Hakozaki, Higashi-ku, Fukuoka 812-8581, Japan; and †NEC Soft, Ltd., 1-18-6, Shinkiba, Koto-ku, Tokyo 136-8608, Japan

ABSTRACT Intermolecular interactions between protein molecules diffusing in various environments underlie many biological processes as well as control protein crystallization, which is a crucial step in x-ray protein structure determinations. Protein interactions were investigated through protein rotational diffusion analysis. First, it was confirmed that tetragonal lysozyme crystals containing fluorescein-tagged lysozyme were successfully formed with the same morphology as that of native protein. Using this nondisruptive fluorescent tracer system, we characterized the effects of sodium chloride and ammonium sulfate concentrations on lysozyme-lysozyme interactions by steady-state and time-resolved fluorescence anisotropy measurements and the introduction of a novel interaction parameter, k_{rot}. The results suggested that the specific attractive interaction, which was reflected in the retardation of the protein rotational diffusion, was induced depending on the salt type and its concentration. The change in the attractive interactions also correlated with the crystallization/precipitation behavior of lysozyme. Moreover, we discuss the validity of our rotational diffusion analysis through comparison with the osmotic second virial coefficient, B_{22}, previously reported for lysozyme and those estimated from k_{rot}.

INTRODUCTION

A precise description of protein interactions in aqueous solution is necessary to understand many biological and biophysical processes in which the collective behavior of proteins are under the control of protein-protein interactions. One such process is protein crystallization, which remains a crucial step in x-ray protein structure determination (1,2). Furthermore, the advancement in treatment of protein condensation diseases, e.g., cataracts and sickle cell anemia (3,4), and the fabrication of nanoscale devices that make use of the self-assembling nature of proteins (5) rely greatly on a clear understanding and proper control of protein attractive interactions.

The osmotic second virial coefficient, B_{22}, is a parameter to characterize protein interactions originated from integration of weak noncovalent interactions such as excluded volume effects, van der Waals attractions, electrostatic repulsions, and hydrophobic and hydration forces (6,7). George and colleagues (8) have demonstrated empirically that a narrow range of slightly negative values of B_{22} observed in dilute protein solutions strongly correlates with the crystallization conditions of globular proteins. Fuelled by this pioneering work, intensive efforts have been directed toward the determination of B_{22} to grasp the feature of protein pairwise interactions by the sedimentation equilibrium method (9), self-interaction chromatography (10,11), and, mainly, optical scattering techniques (12–20). Dynamic light scattering (DLS) measurements, generally used as a diagnostic tool for protein crystallization (21), demonstrate that the protein concentration dependence of the translational diffusion coefficient is used to estimate B_{22} (12,15,16). Underlying this approach is the assumption that a spatial gradient in the chemical potential, which is closely linked to osmotic pressure, is the driving force for the translational diffusion of protein in solution (16,22–24). In this way, the measurement of protein translational diffusion has disclosed protein interactions via B_{22}.

Yet, protein rotational diffusion rarely has been used as an indicator for investigating protein interactions. Whereas translational diffusion can be described from movement in a spatial distance, rotational diffusion can be defined in terms of a spatial orientation angle (23), thus reflecting more microscopic changes in the physicochemical nature of protein including protein size, shape, and hydration state (25,26). Furthermore, the protein rotational motion is essential for the ordering process of protein molecules, i.e., protein crystallization. In this context, the investigation of protein rotational diffusion in interacting systems is expected to deepen our understanding of protein interactions. This study, therefore, is aimed at examining molecular interactions of lysozyme by rotational diffusion analysis, as is the case with translational diffusion (12,15,16). Toward this end, we conducted fluorescence anisotropy measurements, which are a prominent optical technique to obtain information on the Brownian reorientation process of fluorophores extrinsically attached to or intrinsically contained in protein molecules, to pursue the rotational diffusion of proteins (27). Moreover, time-resolved anisotropy measurements can differentiate the entire rotational motion of protein molecules and the fast segmental motions around a fluorophore. To date, the application of this method has been limited to a few studies on protein interactions associated with crystallization (28–31). This is due to the undesirable effects on fluorescence caused

Submitted May 1, 2007, and accepted for publication January 23, 2008.

Address reprint requests to Shoji Yamashita, Tel./Fax: 81-92-642-4425, E-mail: yamashita@brs.kyushu-u.ac.jp.

Editor: Marcia Newcomer.

0006-3495/08/06/4484/09 $2.00

doi: 10.1529/biophysj.107.111872

by concentrated protein molecules, which include multiple light scattering, resonance energy transfer, and the reabsorption of emitted photons. As a way to overcome the intrinsic disadvantage of the fluorescence method described above, we examined a small quantity of fluorescent-labeled lysozyme as a tracer in native lysozyme solution. Rigorous investigation by Forsythe and colleagues (32) has shown that a small amount of fluorescent-labeled tracer molecules ($\leq$1.0%) has no marked effects on the crystallization of model proteins such as lysozyme. Their results support the validity of the addition of fluorescent tracer molecules to examine protein interaction related to crystallization.

In this study, we used this fluorescent-labeled system to characterize the effects of sodium chloride and ammonium sulfate concentrations on lysozyme-lysozyme interactions by applying steady-state fluorescence anisotropy measurements and introducing an interaction parameter, which is analogous to the one used for translational diffusion (12,15,16). Moreover, the direct measurement of the rotational diffusion coefficient, D_{rot}, of lysozyme and the differentiation of contribution from rapid depolarizing motion around the lysozyme N-terminal region were conducted with the time-resolved fluorescence anisotropy technique. In addition, we assessed the validity of the interaction parameter obtained from rotational diffusion analysis through comparison with the osmotic second virial coefficient, B_{22}.

MATERIALS AND METHODS

Protein and chemicals

Hen egg white lysozyme (molecular weight of 14,307), six times crystallized, was obtained from Seikagaku (Tokyo, Japan), lacking impurities such as ovalbumin (33). Fluorescein isothiocyanate isomer I (FITC; molecular weight of 389) was purchased from Sigma-Aldrich (St. Louis, MO). Sodium chloride (NaCl; Sigma-Aldrich) and ammonium sulfate ($(NH_4)_2SO_4$; Wako, Osaka, Japan), used as precipitating agents, were of analytical grade, and all other chemicals were of reagent grade. All experiments were conducted in NaAc buffer (100 mM sodium acetate, pH 4.5) prepared with distilled water from a Milli-Q water purification system (Millipore, Billerica, MO), except for FITC-labeling experiments. Lysozyme, NaCl, and $(NH_4)_2SO_4$ were dissolved into this buffer to the required concentration after filtering through a 0.22-μm sterile filter (Millipore). Lysozyme and FITC concentrations were determined by absorbance measurements using the extinction coefficient of 2.64 ml mg^{-1} cm^{-1} at 280 nm for lysozyme (34), and the molar extinction coefficient of 68,000 M^{-1} cm^{-1} (pH 8.0) at 494 nm for FITC.

Labeling of N-terminal amine of lysozyme with FITC

The covalent linking of FITC to the N-terminal amino group of lysozyme and determination of the degree of labeling were performed using the experimental guidelines of Brinkley (35). FITC adjusted to 100 mM in anhydrous dimethyl sulfoxide was added drop by drop to 10 ml of 2 mg/ml lysozyme solution in 100 mM sodium phosphate buffer (pH 7.5) containing 3% dimethyl sulfoxide as a cosolvent to keep the molar ratio of FITC/lysozyme = 5. After this conjugation reaction was conducted in an ice water bath, the reaction mixture was stirred in the dark overnight (>10 h) at 4°C to improve the selectivity of FITC binding to the N-terminal amino group. Unconjugated FITC was removed by gel filtration chromatography on a HiPrep 26/10 desalting column (GE Healthcare, Buckinghamshire, England) equilibrated with 10 mM sodium phosphate buffer (pH 6.5), followed by extensive dialysis. The sample solution was applied to cation-exchange chromatography (HiPrep 16/10 CM-Sepharose; GE Healthcare) by elution with a 0 to 0.5 M NaCl linear gradient. As a result, FITC-labeled and unlabeled lysozyme molecules were separated, and the dye/protein ratio in the FITC-labeled lysozyme (F-lysozyme) was determined to be ~0.8 by absorbance measurements at 280 and 494 nm. F-lysozyme was then concentrated to the desired final concentration by centrifugation with a Centricon YM-3 (Amicon, Beverly, MA) after dialysis against NaAc buffer and filtration through a 0.22-μm sterile filter, and kept frozen at −80°C until use.

Crystallization of lysozyme and F-lysozyme

Crystallization of lysozyme with and without the coexistence of a small amount of F-lysozyme was carried out using the batch method at 20°C in 96-well microplates to assess the effect of F-lysozyme added on the crystallization/precipitation behavior of lysozyme. Three types of solutions were prepared at a fixed concentration of 60 mg/ml by mixing predetermined amounts of lysozyme and F-lysozyme. One solution consisted of only lysozyme; the other two solutions contained 0.1% and 1% F-lysozyme, respectively. These protein solutions and the precipitant medium containing various concentrations of NaCl or $(NH_4)_2SO_4$ in NaAc buffer were mixed at a ratio of 1:1, giving a final protein concentration of 30 mg/ml. Paraffin oil obtained from Hampton Research (Laguna Niguel, CA) was used to prevent batch solution from evaporating.

Fluorescence anisotropy measurements

Steady-state fluorescence anisotropy measurements were carried out at 20°C ± 1°C on a fluorescence spectrophotometer (HITACHI 850; Hitachi, Tokyo, Japan) equipped with two polarizers for excitation and fluorescence detection.

Time-resolved fluorescence anisotropy decay data were collected using a time-correlated single photon counting technique with subpicosecond laser–microchannel plate-based instrumentation. The excitation pulse was generated from a mode-locked Ti:Sapphire pulse laser (Tsunami; Spectra-Physics, Mountain View, CA) pumped by a green-dye laser (Millennia Xs; Spectra-Physics) operating at a repetition rate of 80 MHz, with a pulse duration full width at half maximum of 100 fs. A frequency-doubled 480-nm pulse (model 3980; Spectra-Physics) was used for FITC excitation. On measurement, the pulse repetition rate was reduced to 800 kHz to avoid pulse pileup during photon counting. Fluorescence emission with vertically polarized excitation was detected by a microchannel plate photomultiplier tube (model 3809U-50; Hamamatsu Photonics, Hamamatsu, Japan). The resultant electronic pulse was transmitted via the constant fraction discriminator (model 935; Ortec, Oak Ridge, TN) and the appropriate delay line to the time-to-amplitude converter (TAC) (model 457; Ortec) as the start signal. Additionally, the trigger pulse was detected and amplified by avalanche photodiodes (model C5658; Hamamatsu Photonics). The output was used as the stop signal for the TAC after being passed through the constant fraction discriminator and the delay line. TAC output, after analog-to-digital conversion, generated the digital signals for the multichannel analyzer (Maestro-32; Ortec). The channel width was set to 11.8 ps/ch, and the data were accumulated in 2048 channels. The ratio of laser pulse/fluorescence photon was > 100:1 for relevant counting. A Glan-Taylor polarizer was placed just behind the sample and set at 0° or 90° for measurement of the desired polarization of $I_{VV}(t)$ and $I_{VH}(t)$ (Eqs. 2 and 3). In all cases, the instrument response function was decided by measuring the scattered light from a diluted polystyrene latex suspension (0.1-μm diameter) and applied for subsequent data analysis. The G-factor was decided to be 1.40 by measuring the intensity ratio of the vertically ($I_{HV}(t)$) and horizontally ($I_{HH}(t)$) polarized emission components of free FITC molecule with horizontally polarized excitation.

Fluorescence anisotropy measurements of F-lysozyme in the solution containing 0.1–20.0 mg/ml of lysozyme and various concentrations of pre-

cipitant (NaCl or $(NH_4)_2SO_4$) were performed while keeping the F-lysozyme concentration constant and dilute (0.03 mg/ml = 2 μM). All measurements were undertaken within 5 min after preparing the sample solution and performed at 20°C using a thermostated cell. During both the steady-state and time-resolved measurements, the emission polarizer was rotated from a vertical to a horizontal orientation to obtain the steady-state values and time-dependent decays of fluorescence anisotropy. F-lysozyme samples were excited at 480 nm and fluorescence emission was detected at 520 nm for both steady-state and time-resolved fluorescence measurements.

Data analysis of fluorescence anisotropy measurements

Steady-state fluorescence anisotropy, r_{ss}, is defined as follows:

$$r_{ss} = \frac{I_{VV} - G \times I_{VH}}{I_{VV} + G \times 2I_{VH}}, \quad (1)$$

where I_{VV} and I_{VH} are the vertical and horizontal fluorescence intensities against the vertical excitation, respectively. G is the polarization bias of the detection instrumentation.

Fluorescence anisotropy decay data were analyzed by means of the nonlinear least-squares iterative convolution method based on the Marquart algorithm (36,37). Diagnosis of the fitting adequacy was done using the statistical parameters such as the sigma value, the serial variance ratio, and plots of weighted residuals. The decays of vertical (I_{VV}) and horizontal (I_{VH}) components, after vertically polarized excitation, were given as follows (27):

$$I_{VV}(t) = \frac{1}{3} I(t)[1 + 2r(t)] \quad (2)$$

$$I_{VH}(t) = \frac{1}{3} I(t)[1 - r(t)]. \quad (3)$$

$I(t)$ and $r(t)$ are the total fluorescence intensity decay and fluorescence anisotropy decay, respectively, which could be described as a sum of exponentials. For relatively simple cases, anisotropy decay can be described by a double exponential function, as follows:

$$r(t) = \beta_L \exp(-t/\phi_L) + \beta_S \exp(-t/\phi_S), \quad (4)$$

where ϕ_L represents the entire rotational correlation time of the protein, and ϕ_S represents the rotational correlation time of fast segmental motion around the fluorophore. β_L and β_S are the preexponential terms related to the amplitude of each rotational motion. The subscripts L and S denote the long and short time components, respectively. Anisotropy decays of F-lysozyme for all measurement conditions were fit using this equation with maximum accuracy. Assuming a spherical shape of the protein molecule, the correlation time for the protein's entire rotation (ϕ_L) is converted to the rotational diffusion coefficient, D^0_{rot}, and is directly related to the hydrodynamic volume of protein (V) temperature (T), and viscosity of the solution (η) by the Stokes-Einstein-Debye relationship, as follows:

$$\phi_L = \frac{1}{6D^0_{rot}} = \frac{\eta V}{kT}. \quad (5)$$

In addition, the freedom of the segmental mobility, f, is given from the relative amplitudes (38), as follows:

$$f = \frac{\beta_S}{\beta_S + \beta_L}. \quad (6)$$

Interaction parameter for protein rotational motion

In a noninteracting system, i.e., at an infinitely dilute protein concentration, steady-state fluorescence anisotropy, r_{ss} (Eq. 1), is related to the rotational diffusion coefficient of protein, D^0_{rot}, and fluorescence lifetime, τ, according to the Perrin equation (39), as follows:

$$\frac{r_0}{r_{ss}} = (1 + 6D^0_{rot}\tau), \quad (7)$$

where r_0 is the initial anisotropy decided only by the angular difference between the absorption and fluorescence transition moments. Crosio and Jullien (28) have expanded this equation to an interacting system and investigated the initial step in the crystallization of ribonuclease A. They anticipated that an apparent rotational correlation time, ϕ_{app}, in the interacting system would deviate from ideality in proportion to the protein concentration, and they introduced an empirical virial coefficient, α, for the rotational mobility. The osmotic second virial coefficient, B_{22}, is directly proportional to the interaction parameters estimated through DLS measurement of the translational diffusion coefficient of macromolecules (12,15,16). There is a reciprocal relationship between the rotational correlation time, ϕ, and the rotational diffusion coefficient, D^0_{rot} (Eq. 5). Therefore, we installed an interaction parameter, k_{rot}, associated with the rotational diffusion coefficient of protein following the case of the translational diffusion coefficient.

At the region of the semidilute protein concentration, an empirical relation between an apparent rotational diffusion coefficient, D_{rot}, and the interaction parameter, k_{rot}, delineating the deviation from the ideality of protein solution behavior, is given as follows:

$$D_{rot} = D^0_{rot}(1 + k_{rot}[C]). \quad (8)$$

In this case, an apparent fluorescent anisotropy value, r_{app}, measured by the steady-state method, is expressed as follows:

$$\frac{r_0}{r_{app}} = (1 + 6D_{rot}\tau). \quad (9)$$

Dividing Eq. 9 by Eq. 7 and combining it with Eq. 8, we obtained equations by which the r_{app}-value measured was linked to the interaction parameter, k_{rot}, as follows:

$$\frac{r_{ss}}{r_{app}} = (1 + l[C]), \quad l = k_{rot}\left(1 - \frac{r_{ss}}{r_0}\right). \quad (10)$$

Using the above relationships, k_{rot}-values under the various precipitant conditions can be estimated from the dependence of r_{app} and D_{rot} on the protein concentration (0–20 mg/ml), which are measured by steady-state and time-resolved measurements, respectively. If the k_{rot}-value is negative, the net interaction has an attractive direction and D_{rot} becomes smaller than D^0_{rot}, and vice versa.

RESULTS

Lysozyme/F-lysozyme crystallization

Using NaCl as a crystallizing agent, no crystals emerged within ~10 h in batch solutions at concentrations lower than 0.5 M. At concentrations between 0.68 and 1.0 M, single crystals of lysozyme with a clear tetragonal morphology were observed for all types of protein solution. Fig.1 shows representative photographs of tetragonal crystals of lysozyme formed in 0.85 M NaCl solution containing 0% (*A*), 0.1% (*B*), and 1% (*C*) F-lysozyme. Under the optical (*upper panel*) and fluorescence (*lower panel*) microscope, no differences in the morphology or size of crystals were found in three types of solution. At NaCl concentrations $>$ 1.4 M, amorphous precipitates were obtained. On using $(NH_4)_2SO_4$ as the precipitant, there were no precipitates or crystals $\leq$ 1 M.

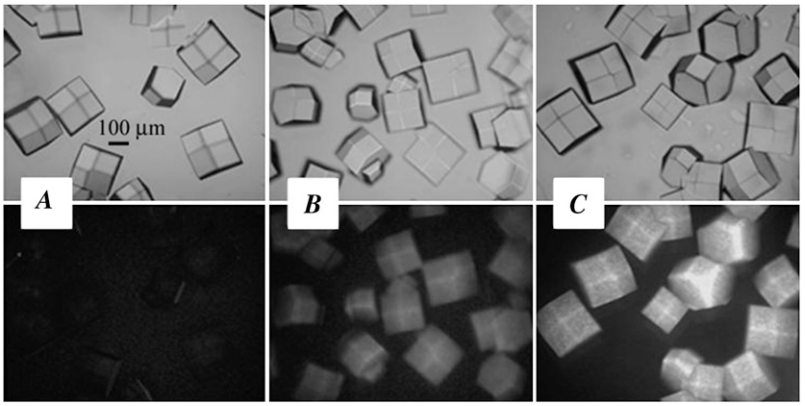

FIGURE 1 Bright field (*upper*) and fluorescence (*lower*) images of crystals of lysozyme (*A*), and lysozyme with different concentrations of fluorescent-labeled lysozyme: (*B*) 0.1% and (*C*) 1%. All crystals were grown by the batch-method with 0.85 M NaCl at 20°C. Fluorescence observation was done with constant laser excitation of 488 nm (10× magnification; incubation time = 5 days).

Amorphous precipitation occurred spontaneously after mixing batch solutions at higher concentrations (1.5 and 1.8 M).

For both cases using NaCl or $(NH_4)_2SO_4$, the addition of a small amount of F-lysozyme did not disrupt lysozyme crystallization and precipitation. These crystallization behaviors, including the time required to crystallize, are in accordance with the lysozyme crystallization and precipitation kinetics mapped to its phase diagram (40). Furthermore, Forsythe and colleagues (32) confirmed visually and by x-ray analysis that the nucleation rate and qualities of lysozyme crystals were not affected by adding labeled protein up to a mixture level of 1%. Two kinds of lysozyme fluorescent derivatives were used in their investigation. One was singly labeled on N-terminal amine, and the other was randomly labeled on ε-amino groups of six lysine residues with a carboxyrhodamine succinimidyl ester (molecular weight of 555.89) (32). Because carboxyrhodamine succinimidyl ester has a larger molecular size and is more hydrophobic than FITC, it is reasonable to conclude that the presence of a trace of F-lysozyme does not affect the crystallization of lysozyme. Thus, protein interactions leading to crystallization are not significantly influenced by the labeling of N-terminal amine of lysozyme with FITC.

Effects of sodium chloride

Steady-state fluorescence anisotropy

Typical results of steady-state fluorescence anisotropy measurements are seen in Fig. 2 *A* as the plot of r_{ss}/r_{app} versus the lysozyme concentration at various NaCl concentrations (0, 0.85, and 1.7 M). When r_{ss}/r_{app}-values were plotted based on Eq. 10, they decreased linearly with an increasing protein concentration, indicating that average rotational motion of F-lysozyme is retarded. The straight solid lines in Fig. 2 *A* produced by least-square fits to the data gave a definitive extrapolated value, which was the anisotropy value in the noninteracting system, r_{ss}. The resulting r_{ss}-values were approximately constant (0.22−0.23). According to Eq. 10, the r_0-value of fluorescein (~0.4) was used to obtain the parameter k_{rot} (41). Fig. 2 *B* depicts the dependence of k_{rot} on the NaCl concentration. In all cases, k_{rot} was negative and decreased monotonically from -0.44×10^{-2} ml/mg at 0 M NaCl to -1.96×10^{-2} ml/mg at 1.7 M NaCl.

These results can be explained by the increase in attractive interactions between lysozyme molecules. George and colleagues (8) assumed that the B_{22}-values representing nonideal behavior in a semidiluted protein solution also reflected intermolecular interactions similar to supersaturated solutions. Based on this assumption, Muschol and Rosenberger (12) demonstrated that the linear relationships in the plots of static light scattering against the protein concentration in the

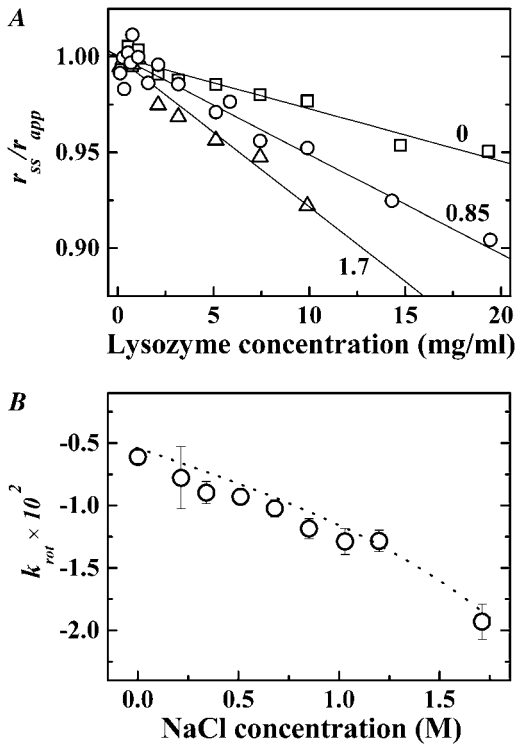

FIGURE 2 Variation of lysozyme interactions with NaCl concentration from steady-state results. (*A*) Effects of increasing NaCl concentration on apparent fluorescence anisotropy of fluorescein-tagged lysozyme. The NaCl concentration is indicated near the line. (*B*) The interaction parameter k_{rot} as a function of NaCl concentration.

lysozyme-NaCl supersaturated region were caused by the changes in intermolecular force rather than by aggregate formation. Also, DLS measurement by Skouri and colleagues (42) showed no larger scatters other than lysozyme monomer in a solution containing 20 mg/ml lysozyme and 3%−5% NaCl. Hence, the persistence of linearity in r_{ss}/r_{app} plots over the wide range of protein concentration (Fig. 2 *A*) suggests that the change in fluorescence anisotropy is caused by protein interactions. Furthermore, the observed downward trend of negative k_{rot}-values with an increasing NaCl concentration indicates that the increment of attractive interactions would be expedited by increasing NaCl content, correlating with the crystallization behavior of lysozyme.

Time-resolved fluorescence anisotropy

We further examined the effect of NaCl on protein interactions through the direct measurement of the rotational diffusion coefficient, $D_{rot,}$ by a time-resolved technique. Fig. 3 *A* shows the vertically (I_{VV}) and horizontally (I_{VH}) polarized emission decays of F-lysozyme with 0.5 mg/ml lysozyme in NaAc buffer at 20°C. By applying the global analysis procedure, the anisotropy decay $r(t)$ could be well fitted to the double exponential kinetics for each condition (Eqs. 2–4). The weighted residuals of the fittings for $I_{VV}(t)$ and $I_{VH}(t)$ are shown in the lower panels of Fig. 3 *A*. The acquired sigma value and the serial variance ratio of $I_{VV}(t)$ and of $I_{VH}(t)$ were 1.03, 1.93, and 1.89, respectively, and a random distribution of residuals could be visually ascertained. Fig. 3 *B* shows the fluorescence anisotropy decay, $r(t)$, of F-lysozyme in 0.5 mg/ml lysozyme. Two rotational correlation times were obtained: $\phi_L = 5.66$ ns ($\beta_L = 0.29$) and $\phi_S = 0.17$ ns ($\beta_S = 0.06$). In addition, anisotropy decay, $r(t)$, was fitted as a sum of two exponential components for all other conditions. According to the Stokes-Einstein-Debye relationships (Eq. 5), the hydrodynamic radius was calculated to be 17.6 Å from the ϕ_L value on the condition of solution viscosity $\eta = 1.0$ cP and 293 K. This value almost corresponds to the equivalent spherical radius of a lysozyme monomer (17.2 Å), estimated from the crystallographic structure of lysozyme, being slightly smaller than that estimated from DLS (19 Å) (12).

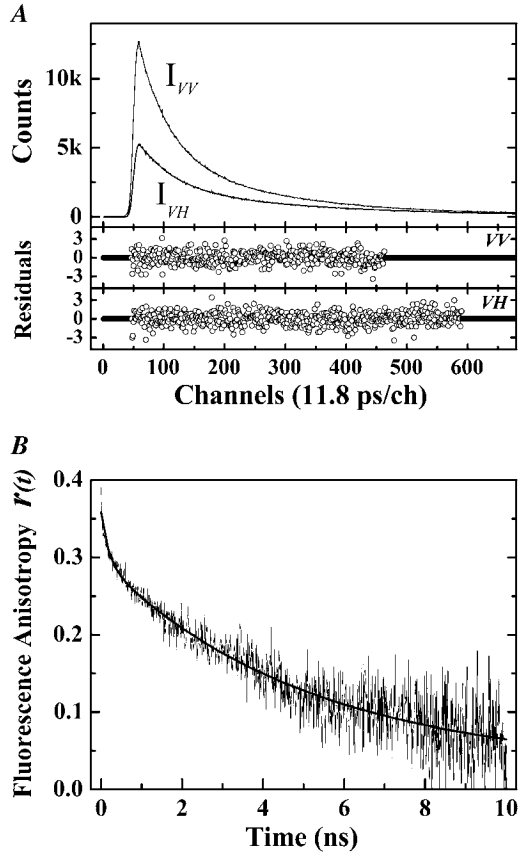

FIGURE 3 Example of time-resolved fluorescence anisotropy measurement results (*A*). (*Upper*) Parallel (I_{VV}) and perpendicular (I_{VH}) emission decay of fluorescein-labeled lysozyme in 0.5 mg/ml lysozyme solutions at pH 4.5. (*Lower*) plots of weighted residuals. (*B*) Time-resolved fluorescence anisotropy decay of fluorescein-labeled lysozyme in 0.5 mg/ml unlabeled lysozyme.

According to Eq. 5, the ϕ_L value is converted to the apparent rotational diffusion coefficient D_{rot}. Linear fitting of D_{rot} plots against the added protein concentration under the presence of NaCl gave intercept values of the rotational diffusion coefficient at an infinite dilution, D^0_{rot}. Through every measurement condition, the obtained D^0_{rot} values converged within the fairly narrow range from 2.7×10^7 s^{-1} to 3.0×10^7 s^{-1}, from which the hydrodynamic radius of lysozyme is determined to be 17.5−18.1 Å. These values of D^0_{rot} also are shown to be in good agreement with the theoretical value (2.8×10^7 s^{-1}) calculated from the realistic structural model assuming actual shape and smoothed surface of the protein (43).

Fig. 4 *A* shows the plots of D_{rot} normalized by D^0_{rot} versus the lysozyme concentration at various NaCl contents. Here, although the plots of D_{rot}/D^0_{rot} in Fig. 4 *A* seemed to be somewhat dispersed, this was within the experimental error on measurements of the rotational correlation time. As also seen in the steady-state results, the entire rotational motion of F-lysozyme was restrained (the rotational diffusion coefficient decreased) as the protein concentration was increased. This tendency was more pronounced with increasing NaCl. Based on Eq. 8, the interaction parameter k_{rot} was directly extracted from the slope of the linear regression of the protein concentration dependence of D_{rot}/D^0_{rot} shown in Fig. 4 *A*. The longest ϕ_L value of 9.80 ns observed in the 10 mg/ml lysozyme solution at 1.7 M NaCl was markedly smaller than that of the lysozyme dimer (16.5 ns) formed at pH 9, derived from magnetic relaxation dispersion data (44). This fact corroborates that no aggregate formation occurs. Additionally, the obtained values of ϕ_L (<9.80 ns) remain confined to the approximate range of the recoverable rotational correlation time (45), $0.1\tau < \phi < 10\tau$, where τ is the probe's fluorescence lifetime. For free FITC, the fluorescence lifetime was determined to be 2.94 ns.

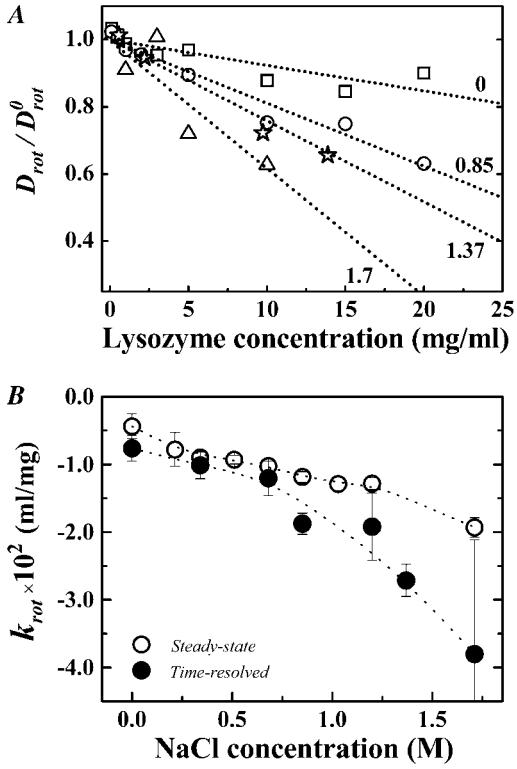

FIGURE 4 Variation of lysozyme interactions with NaCl concentration obtained from time-resolved fluorescence anisotropy measurements. (*A*) Normalized rotational diffusion coefficient $D_{\rm rot}/D^0_{\rm rot}$ versus lysozyme concentration with added NaCl in NaAc buffer at 20°C. Dotted lines represent the linear fits against each plot. The NaCl concentration is indicated near the line. (*B*) NaCl concentration–dependence of the interaction parameter $k_{\rm rot}$ from the time-resolved experiment (*solid circle*). The $k_{\rm rot}$ values from steady-state measurement (see Fig. 2 *B*) are rescaled and plotted for comparison (*open circle*).

Fig. 4 *B* compares the variation of $k_{\rm rot}$ with increasing NaCl concentrations with the $k_{\rm rot}$ variation obtained by steady-state measurement. The monotonic decrease of $k_{\rm rot}$ indicates the increment of attractive interactions induced by NaCl, where the negative $k_{\rm rot}$ goes from -0.76×10^{-2} ml/mg at 0 M NaCl to -3.8×10^{-2} ml/mg at 1.7 M NaCl. The correlation between lysozyme crystallization and the slightly negative $k_{\rm rot}$-values demonstrated here is closely analogous to the crystallization slot of B_{22} proposed by George and colleagues (8). Also, the marked difference in the strength of interaction between the steady-state and time-resolved results is seen at a higher concentration of NaCl. Because steady-state fluorescence anisotropy measures averaged Brownian reorientational motions over the overall protein rotational motion and segmental fluctuation, the disagreement seen in Fig. 4 *B* suggests that the contribution from fast segmental motion on the steady-state anisotropy values presumably becomes larger as the NaCl concentration increases. However, the uncertainty regarding the measurement of a shorter rotational correlation time, $\phi_{\rm S}$ (<500 ps), and the freedom of the lysozyme N-terminal motion, f (Eq. 6), precludes any definite conclusions on that point. Further detailed investigations must be conducted for the correct interpretation of the segmental motion affected by microscopic changes in the surrounding environment. In addition, unfavorable effects of the large segmental flexibility of protein on its crystallizability also have been explored through molecular engineering (46,47). In this case of lysozyme/F-lysozyme crystallization, however, such unfavorable effects were not confirmed. This is probably due to the mobility of the lysozyme N-terminal region being limited, to some extent, by the disulfide bond between Cys 6 and Cys 127. At this time, the assumption of Eq. 8 demonstrates that the differentiation of the depolarizing factor resulting from the rapid, localized motion of the lysozyme N-terminus leads to the precise description of the intermolecular interaction if the entire rotational motion of F-lysozyme is used as its indicator.

Effect of ammonium sulfate

To examine the difference between protein interactions leading to crystallization and those leading to amorphous precipitation, the effects of ammonium sulfate, which is one of the most commonly used salts for protein precipitation, were investigated in a manner similar to that described above. To our knowledge, no lysozyme crystals are obtained from $(NH_4)_2SO_4$ at an acidic pH without modified conditions (48–50). The observed apparent fluorescence anisotropy values, $r_{\rm ss}$, ranged from 0.243 to 0.327, being considerably higher than those obtained in the presence of NaCl (0.223−0.251). For every condition, the anisotropy decay, $r(t)$, was well described as a sum of two exponential components ($\phi_{\rm L}$ and $\phi_{\rm S}$).

The plots of $r_{\rm ss}/r_{\rm app}$ and $D_{\rm rot}/D^0_{\rm rot}$ against the protein concentration showed linear relationships. The interaction parameter $k_{\rm rot}$ is shown in Fig. 5. Unlike in the case of NaCl, steady-state and time-resolved measurements yielded almost the same results. This is because the segmental dynamics affecting the steady-state anisotropy measurement is inde-

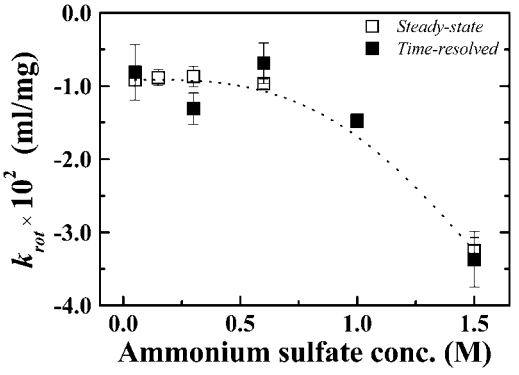

FIGURE 5 Interaction parameter $k_{\rm rot}$ as a function of the ammonium sulfate concentration (M) measured by steady-state (*open square*) and time-resolved fluorescence anisotropy measurement (*solid square*). The dotted line is only a guide for the eye.

pendent of $(NH_4)_2SO_4$ and lysozyme concentrations. At $(NH_4)_2SO_4$ concentrations < 0.6 M, the k_{rot}-values remain almost constant (-0.76×10^{-2} to -0.97×10^{-2} ml/mg), indicating that the attractive interaction would not be induced. At increased concentrations of $(NH_4)_2SO_4$, the values of k_{rot} decrease steeply, illustrating that a marked increase of the attractive interaction occurs. Likewise, in the case of NaCl, the amorphous formation followed the change in k_{rot}.

DISCUSSION

As mentioned above, fluorescence anisotropy studies consistently demonstrated that the rotational motion of F-lysozyme was retarded with increasing lysozyme concentration (Figs. 2 *A* and 4 *A*). This tendency also was pronounced with increasing salt concentration, which was reflected in the decrease in the interaction parameter k_{rot} (Figs. 2 *B*, 4 *B*, and 5). At high salt concentrations, salting-out effects would be induced. In the salting-out process, the screening of Coulombic electrostatic repulsion and dehydration at the protein surface by added salts are complexly intertwined to produce short-range, strong attractive interactions. The observed decrease of the rotational diffusion coefficient of F-lysozyme probably is caused by the attractive interaction between lysozyme molecules. However, close examination is required to determine if some physicochemical factors could affect the rotational motion of protein.

For NaCl, the effect of chloride-ion binding on the protein interactions and the solution restructuring at the ion-binding site has been shown to be small (51,52). Therefore, a possible factor for the cause of decreasing trends of r_{ss}/r_{app} and D_{rot}/D^0_{rot} (Figs. 2 *A* and 4 *A*) is the viscosity increment brought about by increasing lysozyme concentrations ($\sim$20 mg/ml). The normalization of the viscosity increase by adding NaCl already has been conducted by dividing D_{rot} by D^0_{rot}. The dependence of D_{rot}/D^0_{rot} on NaCl should be considered, given that added lysozyme molecules mutually interact under the respective NaCl concentration conditions. The addition of these molecules also increases a peculiar frictional resistance to the rotational mobility of F-lysozyme, resulting in the attractive interaction. This resistance is possibly related to the changes in hydration state of the protein surface. The accurate description of those effects relating to the protein hydration, however, require other specific techniques, such as the femtosecond fluorescence up-conversion method combined with strict theoretical analysis (53,54), and is a key problem to be solved in the future.

Regarding the case of $(NH_4)_2SO_4$, formation of the lysozyme-sulfate ion complex may increase the hydrodynamic radius of F-lysozyme and, thus, cause the decrease in D_{rot}. It has been proposed from light scattering studies that the increased binding of sulfate ions to the lysozyme surface at a low pH significantly induces the repulsive interaction of lysozyme (55). It is highly probable that our observation experimentally supports this assumption from the standpoint of protein rotational dynamics in a concentrated salt solution. The similar decrease of r_{ss}/r_{app} and D_{rot}/D^0_{rot} in 0.05–0.6 M of $(NH_4)_2SO_4$ may reflect combined effects of the enlargement of the hydrodynamic radius of F-lysozyme by ion binding with the increase of frictional resistance, resulting in the constant k_{rot}-values (Fig. 5). It would be reasonable to suppose that such constant k_{rot} values can be regarded as competition among the increased repulsion force induced by water restructuring around bound sulfate ions and the attractive interaction by the salting-out effects.

To assess the validity of the interaction parameter k_{rot} presented here, and to deepen our understanding of protein interactions that are characterized by the changes in protein rotational diffusion, we compared the B'_{22} value that was estimated from k_{rot} (described below) with the osmotic second virial coefficient B_{22} that has been measured previously for lysozyme (14,56). To our knowledge, no theoretical explanations have been established to relate the osmotic second virial coefficient to the protein rotational motion and the interaction parameter k_{rot}. This is because the rotational diffusion is described in terms of the spatial angular difference and is not influenced by a change in the physical environment (23). It is unclear how the chemical potential affects the rotational diffusion of macromolecules in solution, whereas translational diffusion is connected to the osmotic second virial coefficient via the Gibbs-Duhem relation (22). Nevertheless, the retardation of the rotational diffusion of F-lysozyme observed here was indeed dependent on the concentration of lysozyme, NaCl, and $(NH_4)_2SO_4$, suggesting the involvement of the chemical potential. Based on this assumption, although it is possible that a more stringent theoretical treatment is required, B'_{22}-values are estimated from k_{rot}-values in a similar manner as in translational diffusion (16) by $B'_{22} = (k_{rot} + \nu)/2M_W$, where ν is the partial specific volume of lysozyme (0.703 ml/g), and M_W is the molecular weight of lysozyme (14,307).

In Fig. 6, B'_{22}-values estimated from k_{rot} were plotted as a function of ionic strength, together with the second virial coefficient B_{22} obtained for the lysozyme-NaCl system (14,56). Interestingly, the B'_{22}-values were found to be in the range from -4.0×10^{-4} to -6.5×10^{-4} ml mol/g^2 at 0.68$-$1.2 M of NaCl, in good agreement with the reported B_{22}-values (14,56), within the crystallization slot (8). Considering the expression used to derive B'_{22} and B'_{22}'s analogy to the translational expression, ($B_{22} = (k_d + \nu)/2M_W$, where k_d is the analogous parameter to k_{rot}) (16), it seems that the rotational diffusion is slowed with increasing protein concentration in a manner similar to translational diffusion at increased NaCl concentrations. In contrast, the discrepancy between B'_{22} and the reported B_{22}-values were confirmed at a low ionic strength. In this regime, B_{22} shows a positive value, being indicative of repulsive interactions. The dependence of D_{rot}/D^0_{rot} on the protein concentration, however, shows a negative slope (0 M NaCl in Fig. 4 *A*), resulting in the negative B'_{22}-value. The osmotic second virial coefficient, B_{22},

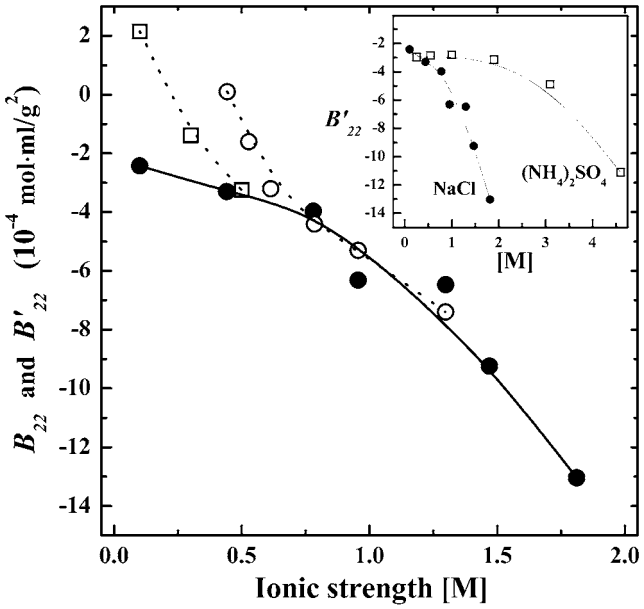

FIGURE 6 Comparison of B'_{22} estimated from k_{rot} values (*solid circle*) and the osmotic virial coefficient B_{22} (*open circle*) from Guo and colleagues (14) and (*open square*) from Velev and colleagues (56), as a function of ionic strength. The inset shows the variation of B'_{22} with ionic strength of different salts, sodium chloride, and ammonium sulfate. The lines are only guides for the eye.

generally represents averaged interaction forces between protein molecules, whereas B'_{22} can be obtained from the changes in protein rotational diffusion being affected by tangential forces exerting a torque on the protein. It is unclear, however, how the averaged force impacts the tangential force. It also has been shown that the rotational diffusion is changed with increasing protein concentration due to solvent-mediated hydrodynamic interactions (57) and/or the long-range electrostatic interactions (58). Thus, a precise interpretation of the result comparing B_{22} and B'_{22} (Fig. 6) requires further investigations and theoretical considerations on the protein rotational diffusion, which has a shorter distance and time scale compared to translation.

In addition, the variation of B'_{22} with ionic strength showed a distinctive behavior depending on the two salt types, NaCl and $(NH_4)_2SO_4$ (Fig. 6, *inset*). There was a marked difference between the ionic strength dependence of B'_{22} for NaCl and that for $(NH_4)_2SO_4$. This indicates that the ability of NaCl to induce attractive interactions is stronger than that of $(NH_4)_2SO_4$ with respect to the increase of ionic strength. Similar results were reported by Curtis and colleagues (55). They pointed out that the attractive force for crystallization required geometrical complementarity or orientation between the protein molecules, whereas the attractive interaction induced by $(NH_4)_2SO_4$ was attributed largely to centrosymmetric osmotic forces, thus triggering the amorphous formation of protein (55). Because the interaction parameter k_{rot} applied here was derived from the protein rotational diffusion, namely reorientational motion, the variation in the attractive interaction with increasing NaCl concentrations may reflect the orientational process in which protein molecules can relax into a suitable orientation for crystallization.

In conclusion, we have shown that the salt-induced attractive interactions can be reliably monitored through the retardation of rotational diffusion, producing the negative k_{rot}-values, as well as that of the translational diffusion. The observed difference of the increasing mode of attractive interaction between the two salts can be meaningfully discussed in terms of the change in hydrodynamic properties of F-lysozyme and is closely related to the lysozyme crystallization or amorphous precipitation. Therefore, it is expected that protein rotational diffusion analysis, combined with translational analysis, will expand our understanding of protein interactions from an integrative standpoint.

REFERENCES

1. Tyers, M., and M. Mann. 2003. From genomics to proteomics. *Nature.* 422:193–197.
2. Hui, R., and A. Edwards. 2003. High-throughput crystallization. *J. Struct. Biol.* 142:154–161.
3. Galkin, O., K. Chen, R. L. Nagel, R. E. Hirsch, and P. G. Vekilov. 2002. Liquid-liquid separation in solutions of normal and sickle cell hemoglobin. *Proc. Natl. Acad. Sci. USA.* 99:8479–8483.
4. Pande, A., J. Pande, N. Asherie, A. Lomakin, O. Ogun, J. King, and G. B. Benedek. 2001. Crystal cataracts: human genetic cataract caused by protein crystallization. *Proc. Natl. Acad. Sci. USA.* 98:6116–6120.
5. McMillan, R. A., C. D. Paavola, J. Howard, S. L. Chan, N. J. Zaluzec, and J. D. Trent. 2002. Ordered nanoparticle arrays formed on engineered chaperonin protein templates. *Nat. Mater.* 1:247–252.
6. Zimm, B. H. 1946. Applications of the methods of molecular distribution to solutions of large molecules. *J. Chem. Phys.* 14:164–179.
7. Neal, B. L., D. Asthagiri, and A. M. Lenhoff. 1998. Molecular origins of osmotic second virial coefficients of proteins. *Biophys. J.* 75:2469–2477.
8. George, A., Y. Chiang, B. Guo, A. Arabshahi, Z. Cai, and W. W. Wilson. 1997. Second virial coefficient as predictor in protein crystal growth. *Methods Enzymol.* 276:100–110.
9. Deszczynski, M., S. E. Harding, and D. J. Winzor. 2006. Negative second virial coefficients as predictors of protein crystal growth: evidence from sedimentation equilibrium studies that refutes the designation of those light scattering parameters as osmotic virial coefficients. *Biophys. Chem.* 120:106–113.
10. Tessier, P. M., A. M. Lenhoff, and S. I. Sandler. 2002. Rapid measurement of protein osmotic second virial coefficients by self-interaction chromatography. *Biophys. J.* 82:1620–1631.
11. Valente, J. J., K. S. Verma, M. C. Manning, W. W. Wilson, and C. S. Henry. 2005. Second virial coefficient studies of cosolvent-induced protein self-interaction. *Biophys. J.* 89:4211–4218.
12. Muschol, M., and F. Rosenberger. 1995. Interactions in undersaturated and supersaturated lysozyme solutions: static and dynamic light scattering results. *J. Chem. Phys.* 103:10424–10432.
13. Bonnetè, F., S. Finet, and A. Tardieu. 1999. Second virial coefficient: variations with lysozyme crystallization conditions. *J. Cryst. Growth.* 196:403–414.
14. Guo, B., S. Kao, H. McDonald, A. Asanov, L. L. Combs, and W. W. Wilson. 1999. Correlation of second virial coefficients and solubilities useful in protein crystal growth. *J. Cryst. Growth.* 196:424–433.
15. Grigsby, J. J., H. W. Blanch, and J. M. Prausnitz. 2000. Diffusivities of lysozyme in aqueous $MgCl_2$ solutions from dynamic light-scattering

data: effect of protein and salt concentrations. *J. Phys. Chem. B.* 104:3645–3650.

16. Zhang, J., and X. Y. Liu. 2003. Effect of protein-protein interactions on protein aggregation kinetics. *J. Chem. Phys.* 119:10972–10976.
17. Narayanan, J., and X. Y. Liu. 2003. Protein interactions in undersaturated and supersaturated solutions: a study using light and x-ray scattering. *Biophys. J.* 84:523–532.
18. Asthagiri, D., A. Paliwal, D. Abras, A. M. Lenhoff, and M. E. Paulaitis. 2005. A consistent experimental and modeling approach to light-scattering studies of protein-protein interactions in solution. *Biophys. J.* 88:3300–3309.
19. Paliwal, A., D. Asthagiri, D. Abras, A. M. Lenhoff, and M. E. Paulaitis. 2005. Light-scattering studies of protein solutions: role of hydration in weak protein-protein interactions. *Biophys. J.* 89:1564–1573.
20. Jia, Y., J. Narayanan, X. Y. Liu, and Y. Liu. 2005. Investigation on the mechanism of crystallization of soluble protein in the presence of nonionic surfactant. *Biophys. J.* 89:4245–4251.
21. Wilson, W. W. 2003. Light scattering as a diagnostic for protein crystal growth—a practical approach. *J. Struct. Biol.* 142:56–65.
22. Harding, S. E., and P. Johnson. 1985. The concentration-dependence of macromolecular parameters. *Biochem. J.* 231:543–547.
23. Tanford, C. 1961. Physical Chemistry of Macromolecules. Wiley, New York.
24. Doi, M., and S. F. Edwards. 1986. The Theory of Polymer Dynamics. Clarendon Press, Oxford.
25. Berne, B. J., and R. Pecora. 1976. Dynamic Light Scattering: With Applications to Chemistry, Biology, and Physics. John Wiley & Sons, New York.
26. Halle, B., and M. Davidovic. 2003. Biomolecular hydration: from water dynamics to hydrodynamics. *Proc. Natl. Acad. Sci. USA.* 100: 12135–12140.
27. Lakowicz, J. R. 1999. Principles of Fluorescence Spectroscopy, 2nd ed. Kluwer Academic/Plenum Publishers, New York.
28. Crosio, M. P., and M. Jullien. 1992. Fluorescence study of precrystallization of ribonuclease A: effect of salts. *J. Cryst. Growth.* 122:66–70.
29. Furuichi, M., E. Nishimoto, T. Koga, A. Takase, and S. Yamashita. 1997. Detergent effects on the light-harvesting chlorophyll A/B-protein complex crystallization revealed by fluorescence depolarization. *Biochem. Biophys. Res. Commun.* 233:555–558.
30. Pan, B., and K. A. Berglund. 1997. Time-resolved fluorescence and anisotropy of covalently coupled 1-pyrenebutyric acid for monitoring the crystallization conditions of lysozyme. *J. Cryst. Growth.* 171:226–235.
31. Collini, M., B. Leo, G. Baldini, H. L. Monaco, and M. Galliano. 2002. Probing protein aggregation by time-resolved fluorescence during β-lactoglobulin crystal growth. *Eur. Biophys. J.* 31:111–117.
32. Forsythe, E., A. Achari, and M. L. Pusey. 2006. Trace fluorescent labeling for high-throughput crystallography. *Acta Crystallogr. D Biol. Crystallogr.* 62(Pt 3):339–346.
33. Thomas, B. R., P. G. Vekilov, and F. Rosenberger. 1996. Heterogeneity determination and purification of commercial hen egg-white lysozyme. *Acta Crystallogrt. D Biol. Crystallogr.* 52(Pt 4):776–784.
34. Aune, K. C., and C. Tanford. 1969. Thermodynamics of the denaturation of lysozyme by guanidine hydrochloride. I. Dependence on pH at 25°. *Biochemistry.* 8:4579–4585.
35. Brinkley, K. 1992. A brief survey of methods for preparing protein conjugates with dyes, haptens, and cross-linking reagents. *Bioconjug. Chem.* 3:2–13.
36. Willis, K. J., and A. G. Szabo. 1989. Resolution of tyrosyl and tryptophyl fluorescence emission from subtilisins. *Biochemistry.* 28: 4902–4908.
37. Zuker, M., A. G. Szabo, L. Bramall, D. T. Krajcarski, and B. Selinger. 1985. Delta function convolution method (DFCM) for fluorescence decay experiments. *Rev. Sci. Instrum.* 56:14–22.
38. Nishimoto, E., S. Yamashita, A. G. Szabo, and T. Imoto. 1998. Internal motion of lysozyme studied by time-resolved fluorescence depolarization of tryptophan residues. *Biochemistry.* 37:5599–5607.
39. Weber, G. 1996. Polarization of the fluorescence of solutions. *In* Fluorescence and Phosphorescence Analysis. D. M. Hercules, editor. Interscience, New York. 217–240
40. Feher, G., and Z. Kam. 1985. Nucleation and growth of protein crystals: general principles and assays. *Methods Enzymol.* 114:77–111.
41. Chen, R. F., and R. L. Bowman. 1965. Fluorescence polarization: measurement with ultraviolet-polarizing filters in a spectrophotometer. *Science.* 147:729–732.
42. Skouri, M., M. Delsanti, J. P. Munch, B. Lorber, and R. Giege. 1991. Dynamic light scattering studies of the aggregation of lysozyme under crystallization conditions. *FEBS Lett.* 295:84–88.
43. Brune, D., and S. Kim. 1993. Predicting protein diffusion coefficients. *Proc. Natl. Acad. Sci. USA.* 90:3835–3839.
44. Gottschalk, M., and B. Halle. 2003. Self-association of lysozyme as seen by magnetic relaxation dispersion. *J. Phys. Chem. B.* 107:7914–7922.
45. Wahl, Ph. 1979. Analysis of fluorescence anisotropy decays by a least squares method. *Biophys. Chem.* 10:91–104.
46. Derewenda, Z. S. 2004. The use of recombinant methods and molecular engineering in protein crystallization. *Methods.* 34:354–363.
47. Derewenda, Z. S., and P. G. Vekilov. 2006. Entropy and surface engineering in protein crystallization. *Acta Crystallogr. D Biol. Crystallogr.* 62(Pt 1):116–124.
48. Rypniewski, W. R., H. M. Holden, and I. Rayment. 1993. Structural consequences of reductive methylation of lysine residues in Hen egg white lysozyme: an X-ray analysis at 1.8-Å resolution. *Biochemistry.* 32:9851–9858.
49. Vuillard, L., T. Rabilloud, R. Leberman, C. B. Colomminas, and S. Cusack. 1994. A new additive for protein crystallization. *FEBS Lett.* 353:294–296.
50. Forsythe, E. L., E. H. Snell, C. C. Malone, and M. L. Pusey. 1999. Crystallization of chicken egg white lysozyme from assorted sulfate salts. *J. Cryst. Growth.* 196:332–343.
51. Curtis, R. A., C. Steinbrecher, M. Heinemann, H. W. Blanch, and J. M. Prausnitz. 2002. Hydrophobic forces between protein molecules in aqueous solutions of concentrated electrolyte. *Biophys. Chem.* 98: 249–265.
52. Grigsby, J. J., H. W. Blanch, and J. M. Prausnitz. 2001. Cloud-point temperatures for lysozyme in electrolyte solutions: effect of salt type, salt concentration and pH. *Biophys. Chem.* 91:231–243.
53. Pal, S. K., J. Peon, and A. H. Zewail. 2002. Biological water at the protein surface: dynamical salvation probed directly with femtosecond resolution. *Proc. Natl. Acad. Sci. USA.* 99:1763–1768.
54. Pal, S. K., and A. H. Zewail. 2004. Dynamics of water in biological recognition. *Chem. Rev.* 104:2099–2123.
55. Curtis, R. A., J. M. Prausnitz, and H. W. Blanch. 1998. Protein-protein and protein-salt interactions in aqueous protein solutions containing concentrated electrolytes. *Biotechnol. Bioeng.* 57:11–21.
56. Velev, O. D., E. W. Kaler, and A. M. Lenhoff. 1998. Protein interactions in solution characterized by light and neutron scattering: comparison of lysozyme and chymotrypsinogen. *Biophys. J.* 75:2682–2697.
57. Bernado, P., J. Garcia de la Torre, and M. Pons. 2004. Macromolecular crowding in biological systems: hydrodynamic and NMR methods. *J. Mol. Recognit.* 17:397–407.
58. Krushelnitsky, A. 2006. Intermolecular interactions and Brownian tumbling in protein solutions. *Phys. Chem. Chem. Phys.* 8:2117–2128.